mathematics

MDPI

Article

Modeling the Kinetics of the Singlet Oxygen Effect in Aqueous Solutions of Proteins Exposed to Thermal and Laser Radiation

Alexey V. Shkirin [1,2], Sergey N. Chirikov [2], Nikolai V. Suyazov [1], Veronika E. Reut [3], Daria V. Grigorieva [3], Irina V. Gorudko [3], Vadim I. Bruskov [4] and Sergey V. Gudkov [1,*]

[1] Prokhorov General Physics Institute of the Russian Academy of Sciences, Vavilova st. 38, Moscow 119991, Russia
[2] Laser Physics Department, National Research Nuclear University MEPhI, Kashirskoe sh. 31, Moscow 115409, Russia
[3] Physics Department, Belarusian State University, 4 Nezavisimosti Av., 220030 Minsk, Belarus
[4] Institute of Theoretical and Experimental Biophysics of the Russian Academy of Sciences, Institutskaya st. 3, Pushchino 142290, Moscow Region, Russia
* Correspondence: s_makariy@rambler.ru

Abstract: A system of kinetic equations describing the changes in the concentration of reactive oxygen species (ROS) in aqueous solutions of proteins was obtained from the analysis of chemical reactions involving singlet oxygen. Applying the condition of the stationarity of the intermediate products to the system, we determined the functional dependence of the hydrogen peroxide concentration on the protein concentration under the action of thermal and laser radiation. An approximate analytical solution to the nonlinear system of differential equations that define the ROS concentration dynamics was found. For aqueous solutions of bovine serum albumin (BSA) and bovine gamma globulin (BGG), the orders and rate constants of the reactions describing the ROS conversions were determined by minimizing the sum of squared deviations of the functions found by solving both the static and dynamic problems from experimentally measured dependences. When solving the optimization problem, the Levenberg–Marquardt algorithm was used.

Keywords: biochemical kinetics; kinetic equations; approximate methods; optimization problems; protein solutions; reactive oxygen species; singlet oxygen effect

MSC: 92C45; 37N25

Citation: Shkirin, A.V.; Chirikov, S.N.; Suyazov, N.V.; Reut, V.E.; Grigorieva, D.V.; Gorudko, I.V.; Bruskov, V.I.; Gudkov, S.V. Modeling the Kinetics of the Singlet Oxygen Effect in Aqueous Solutions of Proteins Exposed to Thermal and Laser Radiation. *Mathematics* **2022**, *10*, 4295. https://doi.org/10.3390/math10224295

Academic Editor: Eugene Postnikov

Received: 18 October 2022
Accepted: 14 November 2022
Published: 16 November 2022

1. Introduction

Modeling the kinetics of biochemical processes can give an understanding of the main formation mechanisms and the roles of the various intermediate and final reaction products (see, for example, [1–3]). More specifically, it helps to assess the influence of external factors (temperature, type of solvent, concentration of the initial components, exposure to ionizing and non-ionizing radiation, etc.), to determine the orders and reaction rates, and to predict the results when changing the type of some of the starting products. In the present work, this kind of mathematical modeling was carried out for reactive oxygen species (ROS) in aqueous solutions of proteins. The term reactive oxygen species (ROS) describes a range of oxygen-derived reactive molecules and free radicals. ROS are constantly formed in aerobic cells as a result of normal metabolism [4] and when exposed to external environmental factors such as ionizing, ultraviolet, extremely high frequency (EHF) microwave radiation [5], plasma [6], xenobiotics [7], thermal exposure [8], and visible and infrared optical radiation [9]. Light exposure (usually by lasers) on biochemical systems leading to the formation of ROS is known as the light-oxygen effect [10–12].

The relevance of this topic is associated, in particular, with the fact that an increase in the intracellular concentration of ROS above a certain level causes "oxidative stress", which is accompanied by damage to biological vital structures, leading to lipid peroxidation, oxidative modification of nucleic acids and proteins, and the disruption of the processes necessary for the life of cells [13,14]. However, it was found that ROS exert not only a damaging effect but also perform a signal-regulatory role in the body associated with a violation of redox homeostasis [15,16]. This leads to the activation of adaptive and protective processes in cells [17,18].

For example, in mammals, a small change in the content of hydrogen peroxide caused by various physical influences may be an important factor in the therapeutic effect and adaptation of the body to adverse environmental conditions [19–21]. A number of physiotherapeutic procedures employing sources of coherent and incoherent light exposure are widely used in medical practice; however, the biological mechanisms of their therapeutic effect are still poorly studied [22]. Under the influence of the electromagnetic radiation of the visible and near-infrared ranges on aqueous solutions saturated with atmospheric oxygen, the formation of ROS (singlet oxygen, superoxide anion radical, hydroxyl radicals, and hydrogen peroxide) is observed [23]. Proteins, due to their high reactivity to oxidation, are the most vulnerable target for ROS compared to lipids, DNA, and other components of biological systems. Oxidation with the help of ROS leads to the loss of the specific functions of proteins, which may be the reason for their destruction and pathological processes leading to aging and the acceleration of its effects [24].

The aim of this work was to construct a kinetic model of the formation of ROS in aqueous solutions of proteins upon irradiation with a heat source and a helium–neon laser at a wavelength of 632.8 nm and then to determine the orders and rate constants for the reactions of formation and decomposition of the ROS by minimizing the sum of squared deviations of the functions found within the kinetic model from the experimentally measured dependences of the hydrogen peroxide concentration on time and the concentration of the dissolved protein in aqueous solutions of BGG and BSA.

To solve the optimization problems when applying the kinetic model to the analysis of the experimental data, the Levenberg–Marquardt method [25–27] was used. The method is based on an iterative procedure for finding the minimum of the objective function in a direction that is a combination of the Newton–Gauss direction and the steepest descent. When the parameters that determine the sum of squared deviations are far from their optimal value, steps are taken practically in the direction of gradient descent, when the parameters are close to their optimal value, in the direction determined by the Newton–Gauss method. Thus, an increase in the step along the gentle slopes of the function and a decrease along the steep descents are achieved, which makes it possible to efficiently find minima even with a ravine relief of the function. The Levenberg–Marquardt method is characterized by increased stability and is less demanding on the initial approximation. The method has quadratic convergence, like Newton's method, if the Jacobi matrix is nondegenerate and Lipschitz continuous. It has become a standard method not only for solving nonlinear least squares problems, but is also widely used in solving other problems, such as in artificial neural networks [28], robotics [29], speech recognition systems [30], optimization of technological processes [31], and algorithms for determining the coordinates and orientation of an object [32]. The method has a disadvantage in that at each step of the iterative process it is necessary, in addition to the gradient of the function, to calculate the Hessian and solve the problem of matrix inversion. This affects the speed of the algorithm when solving multi-parameter (with more than a hundred parameters) problems. The impossibility of approximating the Hessian in terms of the Jacobian in the case of large residuals also reduces the performance of the algorithm. Some modified versions of the Levenberg–Marquardt method have been developed: a modified method with cubic convergence [33]; a high-order Levenberg–Marquardt method, which has biquadratic convergence [34]; a fourth-order method, which is called the accelerated modified

Levenberg–Marquardt method [35]; and a three-step Levenberg–Marquardt (TSLM) algorithm based on fuzzy logic theory (FLT) [36]. However, the modified methods require a large amount of computation, which reduces the advantage of the Levenberg–Marquardt algorithm. When solving problems with a small number of parameters, the method gives excellent results, which is confirmed by its approbation on a number of standard test functions.

2. Materials and Methods

2.1. Mathematical Algorithm

The approach to determining the orders and rate constants of the reactions is as follows. The experimental data were approximated by a model function $f(x, \mathbf{b})$ depending on m parameters $\mathbf{b} = (b_1, \ldots, b_m)$, which is a solution to the system of kinetic equations. The parameter vector was found by minimizing the functional:

$$\Phi(\mathbf{b}) = \frac{1}{2}\sum_{i=1}^{m}(y_i - f(x_i, \mathbf{b}))^2, \quad (1)$$

where (x_i, y_i) are the coordinates of the experimentally measured points. When searching for the minimum of the functional in accordance with the Levenberg–Marquardt method [25–27], the step at the *k*-th iteration is carried out in the direction of the vector $\mathbf{h}$:

$$\mathbf{h} = -(H + \lambda \cdot \mathrm{diag}[H])^{-1} \cdot \nabla\Phi\left(\mathbf{b}^{(k)}\right), \quad (2)$$

where H is the Hessian, which, for small values of the residual, can be expressed in terms of the Jacobian J:

$$H(\mathbf{b}) = J(\mathbf{b})^T \cdot J(\mathbf{b}), \quad (3)$$

where the criterion for the end of the iterative procedure was the increase in the norm of the residual vector by a value not exceeding 10^{-8} of its value at the next step.

2.2. Physical Experiment Protocol

The experimental data on the concentration of hydrogen peroxide in the protein solutions were obtained according to the following protocol. To prepare samples of the protein aqueous solutions, BSA and BGG (Sigma Aldrich, St. Louis, MO, USA) and distilled water (Merck Millipore, San Francisco, CA, USA) were used. Thermal and laser radiation exposure of the samples was carried out with the aid of a U-10 liquid ultrathermostat (Prüfgeräte-WerkMedigen, Berlin, Germany) and a helium–neon laser with a wavelength of 632.8 nm and a power of 3 mW, respectively. The concentration of hydrogen peroxide was measured by enhanced chemiluminescence using a setup (Figure 1) described in detail earlier [24].

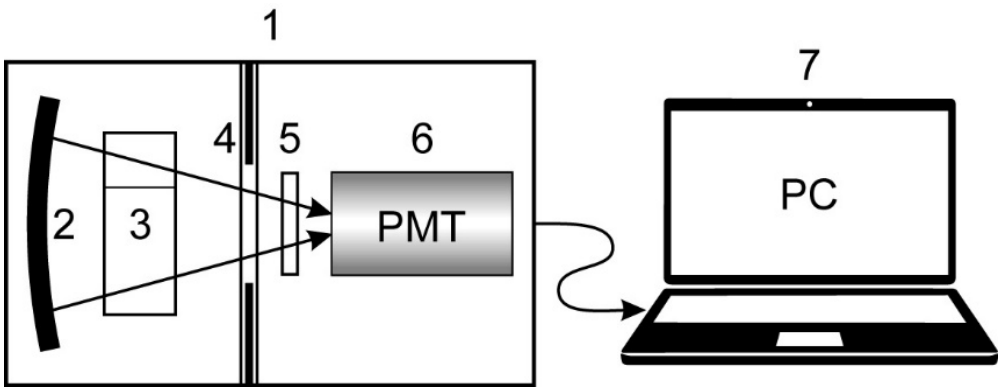

Figure 1. Scheme of the setup for measuring chemoluminescence of protein solutions: (1) Biotox-7A chemoluminometer; (2) focusing mirror; (3) cell with protein solution; (4) photo shutter; (5) optical filter; (6) photomultiplier tube; (7) personal computer.

For the comparison of the thermal and laser effects, two experimental protocols were used: the first was to study the dependence of the hydrogen peroxide concentration on the protein concentration, and the second was to study the time dependence of the hydrogen peroxide concentration. In the first case, aqueous solutions of BGG and BSA at each concentration in the range of 0.1–25 μM were exposed separately to moderate thermal irradiation at 40 °C for 2 h or to laser radiation for 30 min, and then, the hydrogen peroxide concentration was measured. In the second case, aqueous solutions of BGG and BSA with concentrations of 2 μM and 10 μM, respectively, were exposed separately to moderate thermal irradiation at 45 °C for 2 h or to laser radiation for 15 min, after which the time dependence of the hydrogen peroxide concentration was recorded for 6 h.

3. Results

3.1. ROS Reactions in Aqueous Protein Solutions

Under the influence of both thermal radiation and a helium–neon laser on aqueous solutions of proteins saturated with atmospheric oxygen, the formation of singlet oxygen occurs, which is accompanied by the generation of ROS [24]. In the absence of protein in an aqueous solution saturated with atmospheric oxygen, singlet oxygen forms under the influence of electromagnetic radiation:

$$O_2 + h\nu \rightarrow {}^1O_2, \quad (4)$$

where $h\nu$ is the energy quantum of the electromagnetic radiation corresponding to the transition of oxygen from the basic triplet to one of the singlet states: $^1\Delta_g$ or $^1\Sigma_g^+$, whose position corresponds to wavelengths of 1269 nm and 763 nm [37]. The state $^1\Sigma_g^+$ is short-lived and quickly relaxes in $^1\Delta_g$. It is important that a transition in collision complexes (dimoles) is possible, $^3\Sigma_g^- + {}^3\Sigma_g^- + h\nu \rightarrow {}^1\Delta_g + {}^1\Delta_g$, with light absorption at a wavelength of ~630 nm (bandwidth of 18 nm), which allows the use of helium–neon laser radiation with a wavelength of 632.8 nm to generate singlet oxygen [10].

When singlet oxygen interacts with hydroxyl and hydrogen ions, hydroxyl, hydroperoxide radical, and hydrogen peroxide are formed [24]:

$$OH^- + {}^1O_2 + H^+ \rightarrow {}^\bullet OH + HO_2{}^\bullet, \quad (5)$$

$$HO_2{}^\bullet + HO_2{}^\bullet \rightarrow H_2O_2 + {}^1O_2, \quad (6)$$

$$^\bullet OH + {}^\bullet OH \rightarrow H_2O_2, \quad (7)$$

The reaction of $^\bullet$OH with a hydrogen atom at the α-carbon atom of the polypeptide chain in the protein molecule P leads to the detachment of the hydrogen atom and the formation of the α-carbon radical [38]:

$$P + {}^\bullet OH \rightarrow P_{C\alpha}{}^\bullet + H^\bullet, \quad (8)$$

As a result of the reaction of the α-carbon radical with singlet oxygen, a peroxyl radical of the protein is formed [11]:

$$P_{C\alpha}{}^\bullet + {}^1O_2 \rightarrow P_{C\alpha}OO^\bullet, \quad (9)$$

Next is the elimination of the hydroperoxide from the peroxyradical protein:

$$2\ P_{C\alpha}OO^\bullet + H^\bullet \rightarrow 2\ P_e + HO_2{}^\bullet, \quad (10)$$

and the additional formation of hydrogen peroxide due to the dismutation of hydroperoxide radicals according to reaction (6). Along with this, when interacting with singlet oxygen, a number of lateral amino acid residues are also modified [39].

If we summarize reactions (8) and (9), we obtain the formation of a protein peroxy radical as a result of the combined action of hydroxyl radicals and singlet oxygen on the protein:

$$P + {}^{\bullet}OH + {}^1O_2 \rightarrow P_{C\alpha}OO^{\bullet} + H^{\bullet}, \quad (11)$$

Peroxyradical protein is a long-lived reactive protein species (LRPS). The further conversion of LRPS is accompanied by the release of hydroperoxide, the dismutation of two molecules of which leads to the formation of hydrogen peroxide:

$$2P_{C\alpha}OO^{\bullet} + P \rightarrow 2P_e + H_2O_2 + {}^1O_2, \quad (12)$$

where P_e is the final product of the conversion of LRPS from the original protein.

However, for the non-monotonic generation of hydrogen peroxide with the participation of LRPS, one more reaction of its decomposition by protein is additionally required:

$$2H_2O_2 + P \rightarrow 2\,H_2O + {}^1O_2, \quad (13)$$

The kinetic model formulated below predicts the existence of reaction (12), which is a non-catalytic form of the catalase activity of all proteins [40].

3.2. Kinetic Model

Taking into account the reactions involving singlet oxygen in protein aqueous solutions (5)–(13), we can describe the hydrogen peroxide generation observed in the experiments by a simplified minimal system of chemical equations:

$$P + {}^1O_2 \xrightarrow{k_1} P_e + HO_2^{\bullet}, \quad (14)$$

$$HO_2^{\bullet} + HO_2^{\bullet} \xrightarrow{k_2} H_2O_2 + {}^1O_2, \quad (15)$$

$$2H_2O_2 + P \xrightarrow{k_3} 2H_2O + {}^1O_2 + P, \quad (16)$$

$$2H_2O_2 \xrightarrow{k_4} 2H_2O + O_2, \quad (17)$$

Reaction (14) describes the formation of the $HO_2^{\bullet}$ radical, which, in turn, leads to the formation of H_2O_2 in accordance with (15). In the proposed model, two channels of peroxide decomposition are considered: decomposition due to the catalase activity of the protein (16) and self-decomposition (17). For the decay reactions, a mismatch of the experimentally determined reaction orders with the formal stoichiometric coefficients is typical; these orders can be both integer and fractional [41]. Therefore, the kinetic equations for the concentrations of ROS ($HO_2^{\bullet}$ and H_2O_2), corresponding to the above system of chemical reactions, can be written in the general form:

$$d[HO_2^{\bullet}]/dt = k_1 \cdot [P] \cdot [{}^1O_2] - 2 \cdot k_2 \cdot [HO_2^{\bullet}]^2, \quad (18)$$

$$d[H_2O_2]/dt = k_2 \cdot [HO_2^{\bullet}]^2 - 2 \cdot k_3 \cdot [P]^{\gamma} [H_2O_2]^{\beta} - 2 \cdot k_4 \cdot [H_2O_2]^{\alpha}, \quad (19)$$

where k_i ($i = 1 \ldots 4$) are the rate constants of the corresponding reactions, and α, β, γ are the orders of the hydrogen peroxide decomposition reactions. The values of α, β, γ are assumed to be determined from the experimental data.

3.3. Stationary Dependences of the Hydrogen Peroxide Concentration on the Protein Concentration in Aqueous Solutions of BSA and BGG

Applying the stationarity condition for the intermediate reaction products to the system (14)–(17), i.e., the equality of profit and loss for H_2O_2 and $HO_2^{\bullet}$, we obtain

for $HO_2^{\bullet}$:

$$k_1 \cdot [P] \cdot [^1O_2] = 2 \cdot k_2 \cdot [HO_2^{\bullet}]^2, \quad (20)$$

for H_2O_2:

$$k_2 \cdot [HO_2^{\bullet}]^2 = 2 \cdot k_3 \cdot [P]^{\gamma} \cdot [H_2O_2]^{\beta} + 2 \cdot k_4 \cdot [H_2O_2]^{\alpha}. \quad (21)$$

After substituting (20) into (21), we have:

$$k_1 \cdot [P] \cdot [^1O_2] = 4 \cdot k_3 \cdot [P]^{\gamma} \cdot [H_2O_2]^{\beta} + 4 \cdot k_4 \cdot [H_2O_2]^{\alpha}. \quad (22)$$

It is known [41,42] that the self-decomposition of hydrogen peroxide (17) has the order of $1 \le \alpha \le 2$. It is reasonable to assume that the decomposition of peroxide by protein (16) is described, similarly to self-decomposition, by the order of peroxide $1 \le \beta \le 2$. The reaction order for the protein in (16) is not known to us in advance; however, it cannot significantly exceed the order of peroxide; so, it makes sense to search for it in the range $1 \le \gamma \le 3$.

The formation of H_2O_2 was experimentally studied under the influence of moderate thermal radiation at 40 °C for 2 h on the BGG and BSA solutions and upon exposure to He–Ne laser radiation for 30 min. The measured dependences of the H_2O_2 concentration on the concentration of BGG and BSA are shown in Figures 2 and 3, respectively.

In order to simplify the derivation of an explicit function for the H_2O_2 concentration from the Equation (22), we set α and β equal to 1, which is typical for the decomposition of peroxide under normal conditions. Then, the dependence of the peroxide concentration on the protein concentration takes the form:

$$[H_2O_2] = \frac{k_1[P][^1O_2]}{4(k_3[P]^{\gamma} + k_4)}. \quad (23)$$

This dependence can be represented as the following function:

$$y(x) = \frac{x}{ax^{\gamma} + b}, \quad (24)$$

$$a = \frac{4k_3}{k_1[^1O_2]}; \quad b = \frac{4k_4}{k_1[^1O_2]}. \quad (25)$$

We searched for the coefficients (a, b, γ) by minimizing the deviations of the function (24) from the experimental data (Figures 2 and 3) using the Levenberg–Marquardt method [25–27]; the found values (a, b, γ) for the BSA BGG aqueous solutions are given in Table 1.

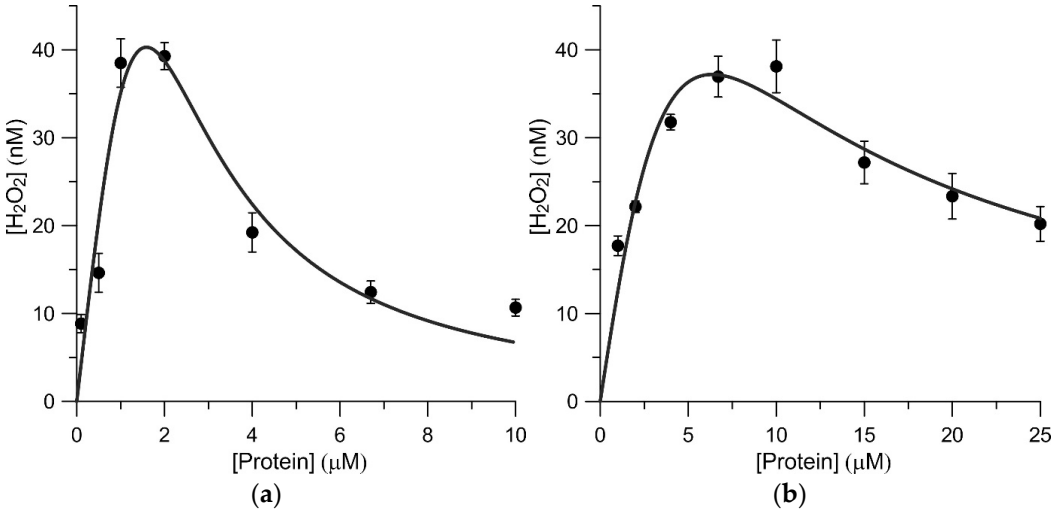

Figure 2. Variation of H_2O_2 concentration with the protein concentration in aqueous solutions exposed to moderate thermal radiation at 40 °C for 2 h: (**a**) BGG; (**b**) BSA. The circles are experimentally measured H_2O_2 concentrations. The solid lines display theoretical approximation of the experimental points by Levenberg–Marquardt method.

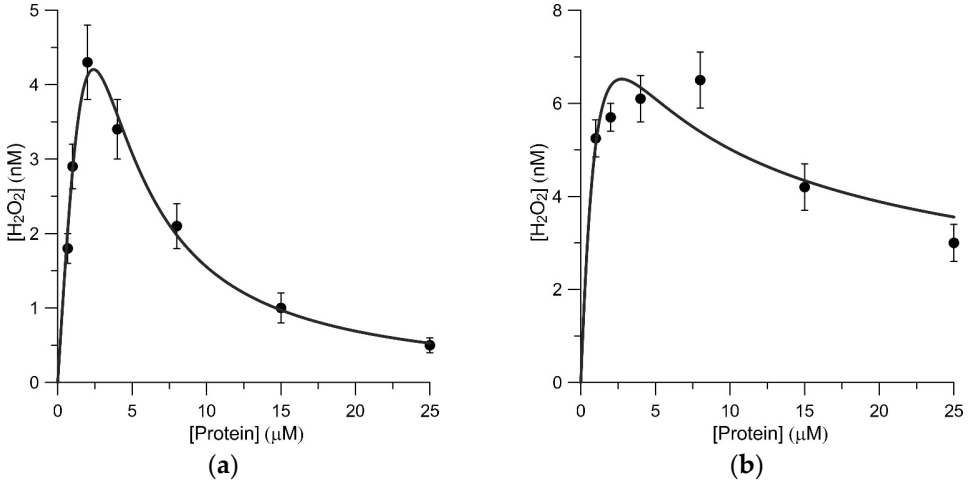

Figure 3. Variation of H_2O_2 concentration with the protein concentration in aqueous solutions exposed to He–Ne laser radiation (3 mW) for 30 min: (**a**) BGG; (**b**) BSA. The circles are experimentally measured H_2O_2 concentrations. The solid lines display theoretical approximation of the experimental points by Levenberg–Marquardt method.

Table 1. Parameters of the model function (24).

Protein	Exposure	a (L²·Micromole⁻²)	b	γ
BGG	Thermal (Figure 2a)	5.17	23.33	2.45
	Laser (Figure 3a)	36.45	315.14	2.23
BSA	Thermal (Figure 2b)	3.32	76.52	1.81
	Laser (Figure 3b)	69.84	125.78	1.43

3.4. Dynamics of Hydrogen Peroxide Formation in Aqueous Solutions of BSA and BGG

Assuming the reaction orders (α, β) are the same as in Section 3.2, we can write the system of kinetic Equations (18) and (19) in the following functional form ($z(t) \equiv [HO_2^{\bullet}]$, $y(t) \equiv [H_2O_2]$) with free coefficients (A, B, C):

$$\frac{d}{dt}z(t) = A - 2Bz(t)^2, \qquad z(0) = z_0, \tag{26}$$

$$\frac{d}{dt}y(t) = Bz(t)^2 - Cy(t), \qquad y(0) = y_0. \tag{27}$$

The time dependence $y(t)$ will have a maximum when the condition $z_0 > \sqrt{\frac{A}{2B}}$ is met. In this case, the solution to system (26), (27) has the form:

$$z(t) = \sqrt{\frac{A}{2B}}\coth\left(\sqrt{2AB}t + \operatorname{arccoth}\left(z_0\sqrt{\frac{2B}{A}}\right)\right), \tag{28}$$

$$y(t) = \frac{A}{2}e^{-Ct}\int_0^t \coth\left(\sqrt{2AB}t + \operatorname{arccoth}\left(z_0\sqrt{\frac{2B}{A}}\right)\right)^2 e^{C\tau}\,d\tau + y_0e^{-Ct}. \tag{29}$$

The search for free coefficients is greatly simplified if (29) is represented through known functions. Replacing $\coth(x)^2$ in the integral (29) for $x > 0$ with an approximate expression $1/x^2 + 1 - e^{-3x/2}/3 - xe^{-53x/60}/2$ (the relative error is no more than $1.3 \cdot 10^{-2}$), we obtain the following function:

$$\begin{aligned} y(t) \cong\ & y_0\exp(-Ct) + \\ +A\Bigg(& \frac{\left(-\frac{\xi\eta_0}{2}+\frac{C}{2}\right)}{\xi\eta_0 C}\exp(-Ct) + \frac{\left(-\frac{1}{2}\mathrm{Ei}\left(\frac{\eta_0 C}{\xi}\right)+\frac{1}{2}\mathrm{Ei}\left(Ct+\frac{\eta_0 C}{\xi}\right)\right)C\exp\left(-Ct-\frac{\eta_0 C}{\xi}\right)}{\xi^2} \\ & + \frac{(900\eta_0 C - 795\xi\eta_0 - 900\xi)\exp\left(-Ct-\frac{53\eta_0}{60}\right)}{(60C-53\xi)^2} + \frac{1}{3}\frac{\exp\left(-Ct-\frac{3\eta_0}{2}\right)}{2C-3\xi} \\ & + \frac{(-15(\xi t+\eta_0)(60C-53\xi)+900\xi)\exp\left(-\frac{53}{60}(\xi t+\eta_0)\right)}{(60C-53\xi)^2} \\ & - \frac{1}{3}\frac{\exp\left(-\frac{3}{2}(\xi t+\eta_0)\right)}{2C-3\xi} - \frac{-\xi^2 t-\xi\eta_0+C}{2\xi(\xi t+\eta_0)C} \Bigg). \end{aligned} \tag{30}$$

Here $\xi = \sqrt{2AB}$, $\eta_0 = \operatorname{arccoth}\left(z_0\sqrt{\frac{2B}{A}}\right)$, and $\mathrm{Ei}(x) = \int_{-\infty}^{x}\frac{e^s}{s}ds$ is the exponential integral. The experimental time dependences of the hydrogen peroxide concentration in the BGG and BSA solutions (concentration 2 μM and 10 μM, respectively) exposed to thermal and laser radiation, as well as the results of their approximation by the Levenberg–Marquardt method using the solution (30), are shown in Figures 4 and 5.

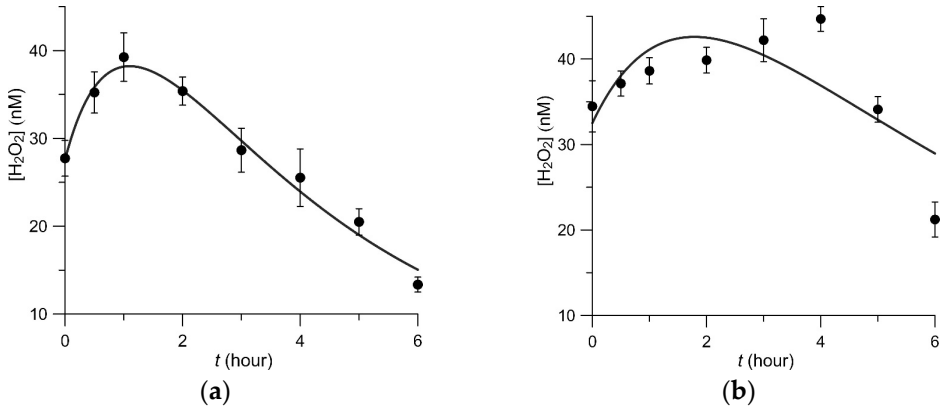

Figure 4. Dynamics of hydrogen peroxide generation in solutions of proteins exposed to heat (45 °C, 2 h) in phosphate buffer (10 mM Na_2HPO_4 and 150 mM NaCl, pH 7.4): (**a**) BGG (2 μM); (**b**) BSA (10 μM). The circles are experimentally measured H_2O_2 concentrations. The solid lines display theoretical approximation of the experimental points by Levenberg–Marquardt method.

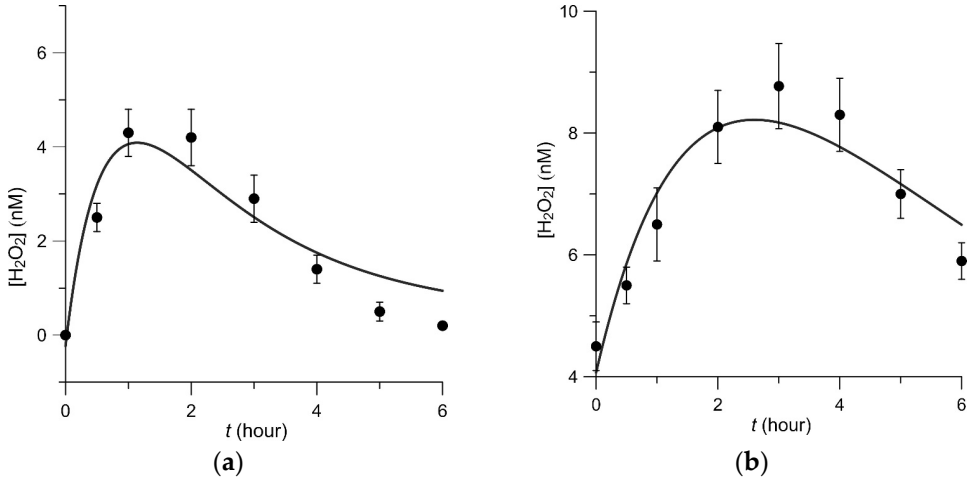

Figure 5. Dynamics of hydrogen peroxide generation in solutions of proteins exposed to laser radiation He–Ne laser (3 mW) for 15 min in phosphate buffer (10 mM Na_2HPO_4 and 150 mM NaCl, pH 7.4): (**a**) BGG (2 μM); (**b**) BSA (10 μM). The circles are experimentally measured H_2O_2 concentrations. The solid lines display theoretical approximation of the experimental points by Levenberg–Marquardt method.

The found parameters of the function (30) in the units indicated on the graphs (Figures 4 and 5) are shown in Table 2.

Table 2. Parameters of the model function (30).

Protein	Exposure	ξ (h^{-1})	η_0	C (h^{-1})	y_0 (nmole·L^{-1})	A (nmole·L^{-1}·h^{-1})
BGG	Thermal (Figure 4a)	0.066	0.136	0.426	0.028	$1.38 \cdot 10^{-3}$
	Laser (Figure 5a)	0.096	0.148	0.939	0.00023	$4.86 \cdot 10^{-4}$
BSA	Thermal (Figure 4b)	0.029	0.163	0.354	0.033	$1.34 \cdot 10^{-3}$
	Laser (Figure 5b)	0.044	0.295	0.396	0.00041	$9.77 \cdot 10^{-4}$

3.5. Chemical Constants

The rate constants for the reactions (14)–(17) are related to the parameters of the functions (24) and (30), which describe the process of hydrogen peroxide generation, by the relations:

$$2(k_4 + k_3[\mathrm{P}]^{\gamma}) = C, \qquad k_3 = \frac{a}{b}k_4, \qquad k_2 = B = \frac{\xi^2}{2\mathrm{A}}, \qquad k_1^{(eff)} = k_1[^1\mathrm{O}_2] = \frac{4k_4}{b}. \tag{31}$$

Having the initially known protein concentrations in the kinetic experiments with BGG ([P] = 2 10 micromole/L) and BSA ([P] = 10 micromole/L), and taking $(a,\ b,\ \gamma)$ from Table 1, we made estimates of the reaction rate constants k_1, k_2, k_3, and k_4 (Table 3), according to (31).

Table 3. Reaction rate constants.

Protein	Exposure	$k_1^{(eff)}$ (s^{-1})	k_2 (L·$mole^{-1}$·s^{-1})	k_3 (L^2·$mole^{-2}$·s^{-1})	k_4 (s^{-1})
BGG	Thermal	$4.6 \cdot 10^{-6}$	$4.4 \cdot 10^{5}$	$5.9 \cdot 10^{6}$	$2.7 \cdot 10^{-5}$
	Laser	$1.07 \cdot 10^{-6}$	$2.6 \cdot 10^{6}$	$9.8 \cdot 10^{6}$	$8.5 \cdot 10^{-5}$
BSA	Thermal	$6.8 \cdot 10^{-7}$	$0.87 \cdot 10^{5}$	$5.6 \cdot 10^{5}$	$1.3 \cdot 10^{-5}$
	Laser	$1.1 \cdot 10^{-7}$	$2.8 \cdot 10^{5}$	$1.9 \cdot 10^{6}$	$3.5 \cdot 10^{-6}$

Note that the found values of k_4 are in an order of magnitude consistent with the interpolated data on the temperature decomposition of hydrogen peroxide [42].

4. Discussion

Considering the effects of singlet oxygen leading to the transformation of LPRS, we determined the minimal system of chemical reactions for ROS conversions in aqueous solutions of proteins and derived the corresponding kinetic equations. By comparison of the obtained kinetic model and the measured dependences of H_2O_2 concentration in BSA and BGG solutions subjected to thermal and laser radiation, we determined the reaction order of the protein-induced decomposition of hydrogen peroxide with respect to the protein and the kinetic constants describing the ROS conversions.

The calculation results (Table 3) show that, compared with laser exposure, under thermal exposure the rate $k_1^{(eff)}$ of the first reaction (14) is several times greater, and the rates k_2, k_3, and k_4 of the subsequent stages (15)–(17) significantly decrease. In contrast with our earlier work, the performed kinetics modeling has an important new feature such that the reaction order with respect to the protein is also included in the set of parameters to be determined using the Levenberg–Marquardt optimization algorithm and, as a result, its value is determined more accurately. Such refinement of the model gives more reliable values of the rates of the intermediate reactions k_j than those obtained with a fixed preset value of the reaction order. The time dependence of the H_2O_2 and $HO_2^{\bullet}$ concentrations derived in an analytical form containing the kinetic parameters is applicable for describing the ROS dynamics in solutions of various proteins under both types of external exposure.

The similarity of the functional dependences of the H_2O_2 concentration on the protein content and time in solutions of the different proteins, both under the action of thermal radiation and the radiation of the He–Ne laser, allowed us to conclude that the fundamental mechanisms of the formation of H_2O_2 are identical in these cases. Thus, similar mathematical approaches can be applied to modeling the ROS conversions in various protein systems, including those that are substantially close to living systems.

5. Conclusions

Hydrogen peroxide is a harmful byproduct of many normal metabolic processes; to prevent damage to cells and tissues, it must be quickly converted into other, less dangerous substances. In this work, we have shown that under thermal/laser irradiation in the visible range, the concentration of protein dissolved in water can serve as a parameter for controlling the decomposition of hydrogen peroxide into the less reactive gaseous molecules of oxygen and water. We have proposed a kinetic model which includes the reaction equation for the catalysis of hydrogen peroxide decomposition due to protein macromolecules. This made it possible to explain the passage of the maximum with the subsequent tending to zero for the experimental dependence of the peroxide concentration on the protein concentration. The dynamics of this process are well described by a system of nonlinear differential equations; good agreement was obtained between the theoretical solution to this system and the experimental measurements.

Author Contributions: Conceptualization, S.V.G., V.I.B., and A.V.S.; methodology, A.V.S., S.N.C., and N.V.S.; software, S.N.C.; validation, V.I.B.; formal analysis, N.V.S.; investigation, V.E.R., D.V.G., I.V.G., A.V.S., S.N.C., and N.V.S.; resources, S.V.G.; data curation, S.N.C.; writing—original draft preparation, A.V.S. and S.N.C.; writing—review and editing, S.V.G.; visualization, S.N.C.; supervision, A.V.S.; project administration, S.V.G.; funding acquisition, S.V.G. All authors have read and agreed to the published version of the manuscript.

Funding: This work was supported by a grant of the Ministry of Science and Higher Education of the Russian Federation (075-15-2022-315) for the organization and development of a world-class research center ''Photonics".

Data Availability Statement: Not applicable.

Conflicts of Interest: The authors declare no conflict of interest.

References

1. Bitsouni, V.; Gialelis, N.; Stratis, I.G. Rigorous Analysis of the Quasi-Steady-State Assumption in Enzyme Kinetics. *Mathematics* **2022**, *10*, 1086. https://doi.org/10.3390/math10071086.
2. Nikolov, S.G.; Wolkenhauer, O.; Nenov, M.; Vera, J. Detection and Analysis of Critical Dynamic Properties of Oligodendrocyte Differentiation. *Mathematics* **2022**, *10*, 2928. https://doi.org/10.3390/math10162928.
3. Sukhinov, A.; Belova, Y.; Nikitina, A.; Sidoryakina, V. Sufficient Conditions for the Existence and Uniqueness of the Solution of the Dynamics of Biogeochemical Cycles in Coastal Systems Problem. *Mathematics* **2022**, *10*, 2092. https://doi.org/10.3390/math10122092.
4. Snezhkina, A.V.; Kudryavtseva, A.V.; Kardymon, O.L.; Savvateeva, M.V.; Melnikova, N.V.; Krasnov, G.S.; Dmitriev, A.A. ROS generation and antioxidant defense systems in normal and malignant cells. *Oxid. Med. Cell. Longev.* **2019**, *2019*, 6175804. https://doi.org/10.1155/2019/6175804.
5. Gapeyev, A.B.; Lukyanova, N.A.; Gudkov, S.V. Hydrogen peroxide induced by modulated electromagnetic radiation protects the cells from DNA damage. *Cent. Eur. J. Biol.* **2014**, *9*, 915–921. https://doi.org/10.2478/s11535-014-0326-x.
6. Piskarev, I. The role of light emission of spark discharge in air in the generation of active species. *High Energy Chem.* **2019**, *53*, 92–93. https://doi.org/10.1134/S0018143919010107.
7. Filev, A.D.; Shmarina, G.V.; Ershova, E.S.; Veiko, N.N.; Martynov, A.V.; Borzikova, M.A.; Poletkina, A.A.; Dolgikh, O.A.; Veiko, V.P.; Bekker, A.A.; et al. Oxidized cell-free DNA role in the antioxidant defense mechanisms under stress. *Oxid. Med. Cell. Longev.* **2019**, *2019*, 1245749. https://doi.org/10.1155/2019/1245749.
8. Bruskov, V.I.; Malakhova, L.V.; Masalimov, Z.K.; Chernikov, A.V. Heat-induced formation of reactive oxygen species and 8-oxoguanine, a biomarker of damage to DNA. *Nucleic Acids Res.* **2002**, *30*, 1354–1363. https://doi.org/10.1093/nar/30.6.1354.
9. Gudkov, S.V.; Bruskov, V.I.; Astashev, M.E.; Chernikov, A.V.; Yaguzhinsky, L.S.; Zakharov, S.D. Oxygen-dependent auto-oscillations of water luminescence triggered by the 1264 nm radiation. *J. Phys. Chem. B* **2011**, *115*, 7693–7698. https://doi.org/10.1021/jp2023154.
10. Zakharov, S.D.; Ivanov, A.V. Light-oxygen effect in cells and its potential applications in tumour therapy. *Quantum Electron.* **1999**, *29*, 1031. https://doi.org/10.1070/QE1999v029n12ABEH001629.
11. Zakharov, S.D.; Ivanov, A.V.; Wolf, E.; Danilov, V.P.; Murina, T.M.; Nguen, K.; Novikov, E.; Panasenko, N.; Perov, S.; Skopinov, S. Structural rearrangements in the aqueous phase of cell suspensions and protein solutions induced by a light-oxygen effect. *Quantum Electron.* **2003**, *33*, 149. https://doi.org/10.1070/QE2003v033n02ABEH002376.
12. Chin, K.K.; Trevithick-Sutton, C.C.; McCallum, J.; Jockusch, S.; Turro, N.J.; Scaiano, J.; Foote, C.S.; Garcia-Garibay, M.A. Quantitative determination of singlet oxygen generated by excited state aromatic amino acids, proteins, and immunoglobulins. *J. Am. Chem. Soc.* **2008**, *130*, 6912–6913. https://doi.org/10.1021/ja800926v.
13. Forman, H.J.; Zhang, H. Targeting oxidative stress in disease: Promise and limitations of antioxidant therapy. *Nat. Rev. Drug Discov.* **2021**, *20*, 689–709. https://doi.org/10.1038/s41573-021-00233-1.
14. Pisoschi, A.M.; Pop, A.; Iordache, F.; Stanca, L.; Predoi, G.; Serban, A.I. Oxidative stress mitigation by antioxidants-an overview on their chemistry and influences on health status. *Eur. J. Med. Chem.* **2021**, *209*, 112891. https://doi.org/10.1016/j.ejmech.2020.112891.
15. Brillo, V.; Chieregato, L.; Leanza, L.; Muccioli, S.; Costa, R. Mitochondrial dynamics, ROS, and cell signaling: A blended overview. *Life* **2021**, *11*, 332. https://doi.org/10.3390/life11040332.
16. Ochoa, C.D.; Wu, R.F.; Terada, L.S. ROS signaling and ER stress in cardiovascular disease. *Mol. Aspects Med.* **2018**, *63*, 18–29. https://doi.org/10.1016/j.mam.2018.03.002.
17. Sharapov, M.; Novoselov, V. Catalytic and signaling role of peroxiredoxins in carcinogenesis. *Biochem.* **2019**, *84*, 79–100. https://doi.org/10.1134/S0006297919020019.
18. Nakamura, H.; Takada, K. Reactive oxygen species in cancer: Current findings and future directions. *Cancer Sci.* **2021**, *112*, 3945. https://doi.org/10.1111/cas.15068.
19. Vlasova, I.I. Peroxidase activity of human hemoproteins: Keeping the fire under control. *Molecules* **2018**, *23*, 2561. https://doi.org/10.3390/molecules23102561.
20. Borisova-Mubarakshina, M.M.; Vetoshkina, D.V.; Ivanov, B.N. Antioxidant and signaling functions of the plastoquinone pool in higher plants. *Physiol. Plant.* **2019**, *166*, 181–198. https://doi.org/10.1111/ppl.12936.
21. Smirnova, O.A.; Bartosch, B.; Zakirova, N.F.; Kochetkov, S.N.; Ivanov, A.V. Polyamine metabolism and oxidative protein folding in the ER as ROS-producing systems neglected in virology. *Int. J. Mol. Sci.* **2018**, *19*, 1219. https://doi.org/10.3390/ijms19041219.
22. Chernov, A.; Reshetnikov, D.; Yu, A.K.; Manokhin, A.; Gudkov, S. Influence of wideband visible light with an padding red component on the functional state of mice embryos and embryonic stem cells. *J. Photochem. Photobiol.* **2018**, *188*, 77–86. https://doi.org/10.1016/j.jphotobiol.2018.09.007.
23. Amaroli, A.; Pasquale, C.; Zekiy, A.; Utyuzh, A.; Benedicenti, S.; Signore, A.; Ravera, S. Photobiomodulation and oxidative stress: 980 nm diode laser light regulates mitochondrial activity and reactive oxygen species production. *Oxid. Med. Cell. Longev.* **2021**, *2021*, 6626286. https://doi.org/10.1155/2021/6626286.

24. Ivanov, V.; Karp, O.; Bruskov, V.; Andreev, S.; Bunkin, N.; Gudkov, S. Formation of long-lived reactive products in blood serum under heat treatment and low-intensity laser irradiation, their role in hydrogen peroxide generation and DNA damage. *Indian J. Biochem. Biophys.* **2019**, 56, 214–223. https://doi.org/10.56042/ijbb.v56i3.27641.
25. Levenberg, K. A method for the solution of certain non-linear problems in least squares. *Q. Appl. Math.* **1944**, *2*, 164–168. https://doi.org/10.1090/qam/10666.
26. Marquardt, D.W. An algorithm for least-squares estimation of nonlinear parameters. *SIAM J. Appl. Math.* **1963**, *11*, 431–441.
27. Nocedal, J.; Wright, S. *Numerical Optimization*; Springer Science and Business Media: New York, NY, USA, 2006.
28. Hua, L.; Bo, L.; Tong, L.; Wang, M.; Fu, H.; Guo, R. Angular Acceleration Sensor Fault Diagnosis Based on LM-BP Neural Network. In Proceedings of the 37th Chinese Control Conference, Wuhan, China, 25–27 July 2018; pp. 6028–6032.
29. Luo, G.; Zou, L.; Wang, Z.; Lv, C.; Ou, J.; Huang, Y. A novel kinematic parameters calibration method for industrial robot based on Levenberg-Marquardt and Differential Evolution hybrid algorithm. *Robot. Comput. Integr. Manuf.* **2021**, *71*, 102165. https://doi.org/10.1016/j.rcim.2021.102165.
30. Kumar, S.S.; Sowmya, R.; Shankar, B.M.; Lingaraj, N.; Sivakumar, S. Analysis of Connected Word Recognition systems using Levenberg Mar-quardt Algorithm for cockpit control in unmanned aircrafts. *Mater. Today Proc.* **2021**, *37*, 1813–1819 https://doi.org/10.1016/j.matpr.2020.07.399.
31. Mahmoudabadi, Z.S.; Rashidi, A.; Yousefi, M. Synthesis of 2D-Porous MoS_2 as a Nanocatalyst for Oxidative Desulfuriza-tion of Sour Gas Condensate: Process Parameters Optimization Based on the Levenberg–Marquardt Algorithm. *J. Environ. Chem. Eng.* **2021**, *9*, 105200. https://doi.org/10.1016/j.jece.2021.105200.
32. Kudinov, I.A.; Pavlov, O.V.; Kholopov, I.S. Implementation of an algorithm for determining the spatial coordinates and the angular orientation of an object based on reference marks, using information from a single camera. *Comput. Opt.* **2015**, *39*, 413–419.
33. Fan, J. The modified Levenberg–Marquardt method for nonlinear equations with cubic convergence. *Math. Comp.* **2012**, *81*, 447–466.
34. Yang, X. A higher-order Levenberg–Marquardt method for nonlinear equations. *Appl. Math. Comput.* **2013**, *219*, 10682–10694. https://doi.org/10.1016/j.amc.2013.04.033.
35. Chen, L. A high-order modified Levenberg–Marquardt method for systems of nonlinear equations with fourth-order convergence. *Appl. Math. Comput.* **2016**, *285*, 79–93. https://doi.org/10.1016/j.amc.2016.03.031.
36. Derakhshandeh, S.Y.; Pourbagher, R.; Kargar, A. A novel fuzzy logic Levenberg-Marquardt method to solve the ill-conditioned power flow problem. *Int. J. Electr. Power Energy Syst.* **2018**, *99*, 299–308. https://doi.org/10.1016/j.ijepes.2018.01.019.
37. Shinkarenko, N.V.; Aleskovskii, V. Singlet oxygen: Methods of preparation and detection. *Russ. Chem. Rev.* **1981**, *50*, 220. https://doi.org/10.1070/RC1981v050n03ABEH002587.
38. Davies, M.J. The oxidative environment and protein damage. *Biochim. Biophys. Acta Proteins Proteom.* **2005**, *1703*, 93–109. https://doi.org/10.1016/j.bbapap.2004.08.007.
39. Davies, M.J. Reactive species formed on proteins exposed to singlet oxygen. *Photochem. Photobiol. Sci.* **2004**, *3*, 17–25. https://doi.org/10.1039/B307576C.
40. Hawkins, C.L.; Davies, M.J. Generation and propagation of radical reactions on proteins. *Biochim. Biophys. Acta Bioenerg.* **2001**, *1504*, 196–219. https://doi.org/10.1016/s0005-2728(00)00252-8.
41. Panchenkov, G.M.; Lebedev, V.P. *Chemical Kinetics and Catalysis*; Khimiya: Moscow, Russia, 1985.
42. Takagi, J.; Ishigure, K. Thermal decomposition of hydrogen peroxide and its effect on reactor water monitoring of boiling water reactors. *Nucl. Sci. Eng.* **1985**, *89*, 177–186. https://doi.org/10.13182/NSE85-A18191